Electromagnetic Characterisation Report on Short Stroke Ferromagnetic Actuators

Omigbodun Tirenioluwa Lois
Email: ye20178@bristol.ac.uk
School Number: U2072442
Course Number: EENG20002

***Abstract*— Engineering characterisation of devices assess the properties of the subject and ascertain its applications. This study examines the electromechanical behaviour of a short-stroke ferromagnetic actuator sample, using analytical and numerical finite element analysis methods. Findings and predictions of the actuator in the electrical, magnetic, and mechanical domains are discussed. It highlights field properties such as Forces, Energy, and Power and the applications of the sample.**

I. INTRODUCTION

The sample depicted in figure 1 is a ferromagnetic actuator with a stator, an armature and two copper windings wound around the stator, both independently energised by a Direct Current source of $10A$ [4]. On excitation of the windings, the stator acts as an electromagnet and attracts the armature in a unidirectional towards it. Motion of the armature is due to the variable air-gap and the fixed air-gaps (0.5mm each).The armature's stroke is 5mm.

Fig. 1. 3-d Image of the Actuator Sample (*extract from reference 4*)

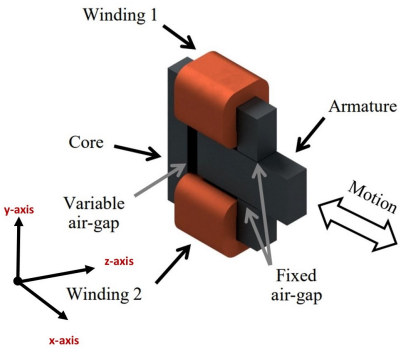

To analyse how the actuator operates, MATLAB aided with Finite Element Method Magnetics (FEMM) software is used in the numerical analysis of the actuator to predict it behaviour.Process illustrated in [4]. Its predictions are compared with the analytical model.

II. METHODOLOGY

Analytical Method of Magnetic Equivalent Circuit: The Magnetic equivalent Circuit (MEC) model uses an analogy that the flux (Φ) flow is similar to the current flow in an electric circuit and the materials of different reluctance properties can be represented by resistances[11,12]. The actuator is represented in a two-dimensional model (2-d) (figure 2), and it is assumed that there are no leakage flux lines i.e the flux path is confined to the actuator cores and air gaps.

Fig. 2. 2-d Image of the Actuator Geometry with Dimensions

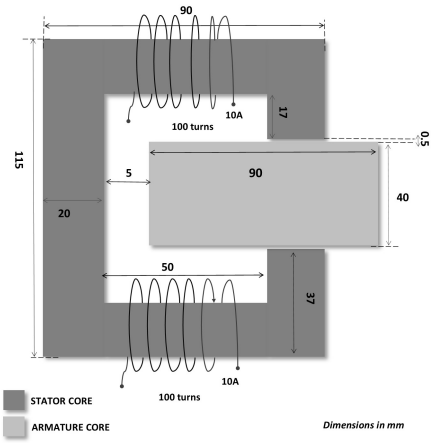

The Actuator windings are excited by two separate sources of same current, $10A$. These generate two flux paths in the cores of approximately equal densities. The 2-d model can therefore be cut (figure 3) to represent the flow of flux from a single winding.The path a,b,c and d represent the mean path of flux flowing through the cores.

Fig. 3. 2-d Image of the Sliced Actuator with Dimensions

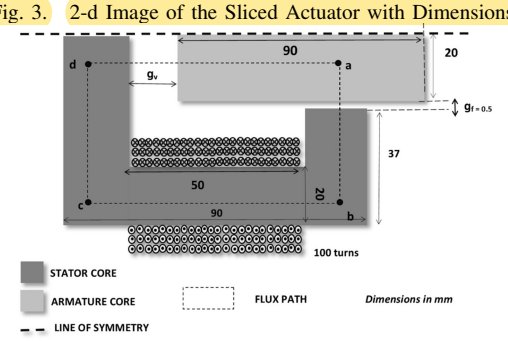

The Reluctance ($\Re$) is dependent on flux. This implies that it depends on the path length (l) of flux, the area it flows through and the properties of the material it flows through.

$$\Re = \frac{l}{\mu_R \mu_o A} \tag{1}$$

where μ_R is the relative permeability,μ_o is the permeability of free space and A is the area. The points a,b,c and d in Figure 3, represents the path flow of flux in the cores. The Magnetic Equivalent circuit is formed as seen in Figure 4. The model uses Ampere's law (2) [11-13] to generate its

Fig. 4. Magnetic Equivalent Circuit

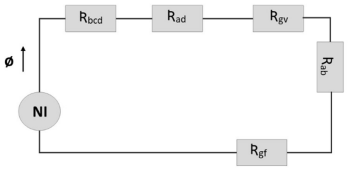

circuit equation (4).

$$MMF = NI = \oint H \cdot dl = \Phi \Sigma \Re \tag{2}$$

where MMF is the Magneto motive force, N is the Number of windings, H is the Magnetic field strength, I is the current and l the length. The sum of Reluctance's in the MEC :

$$\Sigma \Re = \Re_{bcd} + \Re_{ad} + \Re_{g_v} + \Re_{ab} + \Re_{g_f} \tag{3}$$

The representation of equation 2 using 3 with respect to path lengths:

$$NI = \frac{\Phi}{\mu_o}[\frac{1}{\mu_R A_c}(l_{bcd} + l_{ad} + l_{ab}) + \frac{g_v}{A_{g_v}} + \frac{g_f}{A_{g_f}}] \tag{4}$$

$A_c = WT$ *where W and T are the depth and breadth of the stator core respectively.*

TABLE I
PARAMETERS AND THEIR VALUES NECESSARY FOR ANALYTICAL MEC

Symbol	Parameter
g_f	Fixed Air-gap
g_v	Variable Air-gap
A_c	Geometric Area of Stator Core
A_{g_v}	Geometric Area Variable Air-gap
A_{g_f}	Geometric Area Fixed Air-gap
A_{effix}	Effective Area Fixed Air-gap
A_{effv}	Effective Area Variable Air-gap

A_{g_v} and A_{g_f} are dependent on air-gap fringing. Fringing flux lines occur when flux flows through paths of different material properties. If the fringing flux is assumed absent, The Area used is the geometric area of the stator core, $A_{g_v} = A_{g_f} = A_c$ [11].

To account for air-gap fringing, The effective areas are used. Table II illustrates the equations for calculating this. Both

TABLE II
CALCULATION OF THE EFFECTIVE AREA.
an extract from reference [4]

Effective Area	Formula used
A_{effix}	$(W + 2g_f)(T + 2g_f)$
A_{effv}	$(W + g_v)(T + g_v)$

formulas differ because of the area through which the flux flows. In fixed gap, flux flows through points a to b in 3. The dimensions of the armature core are greater than the stator through this path [11]. However, the variable air-gap has equal lengths dimensions as flux flows through points d to a in 3). The dimensions of the stator are used in both equations.

Numerical Method of Finite Element Analysis: FEMM uses a set of boundary and meshing conditions to numerically solve properties of the ferromagnetic actuator [1]. The Numerical analysis method uses **elliptic** representations of Maxwell's Equations to quantitatively analyze the blocks [4] and predict their behavior in the field domains [5].

The following set of assumptions for the numerical analysis of the ferromagnetic actuator using FEMM [3-5]:

1) The problem is solved using a 2-d magneto-statics model. The actuator model has a $20mm$ depth into the plane.
2) The magnetic scalar potential A exists out of page only on the z-plane.
3) The problem is quasi-static.
4) The regions / blocks are uniformly homogeneous.

The boundary conditions are **seven isotropic elliptic shells** approximated by Improvised Asymptotic Boundary Conditions (IABCs) as seen in figure 5. They use Partial Differential Equations of the Maxwell's Equations [8-10] to numerically solve problems within them. They are necessary to limit the number of solutions in the model and also represent an intermediary between the bounded and unbounded region. This is done by reproducing the impedance of an unbounded region for low-order harmonics [10].

The two-dimensional model can be discretised by Delaunay triangulation to generate mesh elements[4,7]. Meshing takes nodal points creating areas where solutions are generated within the allocated boundary. These form triangular mesh elements in boundaries of different material properties and along the edges of each region. Mesh refinement is necessary to ensure an increase in the quality and density of mesh elements. $Smartmesh$, a tool in FEMM which improves the quality of meshing but is quite limited [4]. Before the smartmesh was on, the number of mesh elements are 24828 and when switched on FEMM takes into account 26498 elements.

The Actuator has both fixed and variable air gaps. To ensure that the numerical solution is more accurate, the variable air gap has to have a higher density of mesh elements. This is

Fig. 5. Illustration of the Actuator FEA Model on FEMM GUI showing flux lines, elliptic shells, mesh, and magnetic density vector .

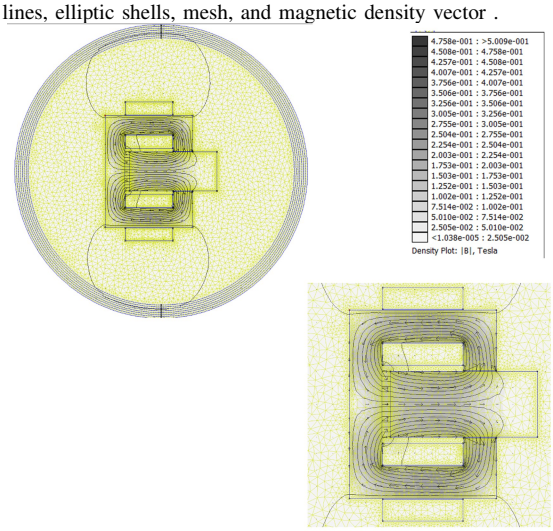

done by manually decreasing the area of each mesh element from 1 to 0.5 and increasing their density. The number of mesh elements increases by 1658 elements. Comparison of both models can be read in section VI.

III. Winding Resistance

The windings in figure 1 are made of copper which has a resistivity. The resistivity of the windings causes there to be a Resistance, which leads to Power dissipation as Heat[11,14]. There are different methods of obtaining the resistance of the windings [5]. The analytical 3-d model, uses the 3-d structure of the actuator to approximate the electrical properties of the winding while the FEA related models use the 2-d structure. Table III illustrates the resistance of a single winding in the actuator model.

TABLE III
Calculation of Winding Resistance

Calculation Model Used	Resistance (Ω)
Analytical 3-d Model	0.0557
FEA Model	0.0107
Analytical FEMM Model	0.0178

The three methods have similarities in implementation but their outputs are different. The FEA Model uses the linear material properties of the windings,i.e., copper, to predict the resistance of the windings. Similarly, both Analytical methods use the electrical conductivity of copper $\sigma = 58MS/m$ in their calculations. Another key feature they all share is the use of the active length (L_{aw}).

L_{aw} is an approximate of the mean path length of current flow and it represents how the electric field generated interacts with a single coil wound around the stator core.

$$L_{aw} = \frac{V_w}{A_w} \tag{5}$$

where V_w is the Volume and A_w is the Cross-sectional Area of the winding block.

Note: The volume and area of the models where extracted from 3d CAD supplied and FEMM properties respectively

Compared to the Analytical 3-d model, both FEA model and Analytical FEMM model have $L_{aw} = 0.040m$ which is less than the 3-d model's L_{aw} of $0.1255m$. The portion of the winding window, that runs in the same plane as the page in FEA model (upper and lower section connectors of each winding) , are not present in the 2-d model but is in the 3-d CAD model[5].

The major distinction between the Analytical models and the FEA model is the packaging factor (k_{pf}). k_{pf} accounts for the geometric packing and spacing of individual coils in the winding block [5]. In the FEA model, the winding block is filled completely with conductor material while the Analytical models assume that the block is 60% filled with conductor material and 40% of air. Since the conductivity (σ) of copper is greater that of air, the resistance of the Analytical FEMM model is greater than the FEA model. The Analytical models use equation 6 to compute the resistance with the packaging factor, where R is the Resistance :

$$R = \frac{NL_{aw}}{\sigma(\frac{k_{pf}A_w}{N})} \tag{6}$$

There are Power losses in the windings due to the windings being energized after armature movement. The Power Losses are calculated using:

$$P_w = IV = I^2R \tag{7}$$

where P_w is the Power loss, V is the Voltage and I the Current. Using the Resistance values in table III, figure 6 shows the winding's power losses plotted as a function of the excitation current in the windings. The power losses in

Fig. 6. Power Loss of the Copper Winding

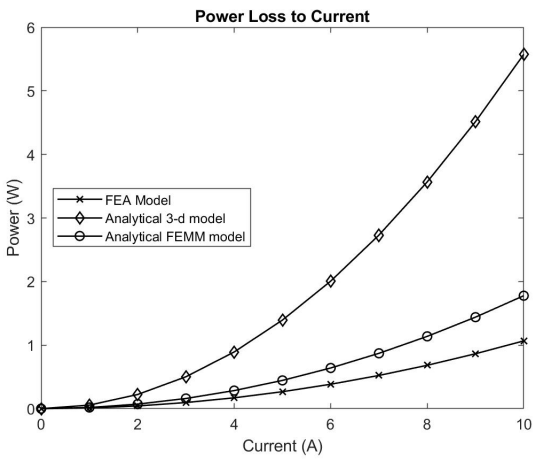

each method increases exponentially with current due to an increase in voltage across the windings i.e Ohms Law. The Analytical 3-d model has a steeper rise compared to other

methods and has the highest power losses. The analytical 3-d model has a winding power loss approximately 70% greater than the FEA model while the Analytical FEMM model is 40% greater at the maximum winding excitation. The power losses in the windings can be reduced by using a shaped profile winding [6]. This reduces the weight of the actuator and make it more applicable in micro-robotics.

IV. Winding Inductance

By means of coupling provided in the conversion of electrical to mechanical energy, Energy is stored in the magnetic field [14]. The stator winding arrangement act as a solenoid which stores energy in its magnetic fields. According Faraday's law and Right-hand grip rule, the N-turn windings links magnetic flux on excitation, as seen in figure 5. The inductance of the solenoid can be calculated.

$$L = \frac{N\Phi}{I} = \frac{N^2}{\Sigma\Re} \tag{8}$$

The equation 8 expresses the inductance in terms of reluctance ($\Re$) and the turns (N). Using the MEC model as illustrated in II, The inductance of the model is represented in terms of the number of turns around the stator and the reluctance of the cores and gaps. Equations 9 and 10 are the inductance equations for when fringing is assumed absent and present respectively.

Fringing absent:

$$L_{nf} = \frac{N^2}{\frac{1}{\mu_o A_c}[g_v + g_f + \frac{1}{\mu_R}(l_{bcd} + l_{ad} + l_{ab})]} \tag{9}$$

Fringing present:

$$L_f = \frac{N^2}{\frac{1}{\mu_o}[\frac{1}{\mu_R A_c}(l_{bcd} + l_{ad} + l_{ab}) + \frac{g_v}{A_{effv}} + \frac{g_f}{A_{effix}}]} \tag{10}$$

The resulting expressions as a function of variable air-gap distance and the values in table IV are seen below.

NOTE: Values are converted to meters in substitution.

TABLE IV
PARAMETERS AND THEIR VALUES NECESSARY FOR ANALYTICAL MEC

Parameters	Value
Number of Turns (N)	100
Depth (W)	$20mm$
fixed gap (g_f)	$0.5mm$
A_c	$400mm^2$
A_{effv}	$(20 + g_v)^2 mm^2$
A_{effix}	$441mm^2$
Length bcd (l_{bcd})	$127.5mm$
Length ab (l_{ab})	$37mm$
Length ad (l_{ad})	$65mm$

Fringing is present:

$$L_f = \frac{10000}{\frac{2500000 g_v}{\pi(g_v^2 + \frac{g_v}{25} + \frac{1}{2500})} + \frac{4268842.12}{\pi}} \tag{11}$$

Fringing is absent:

$$L_{nf} = \frac{16\pi}{10000000 g_v + 7295} \tag{12}$$

The FEMM model has flux lines passing through its cores and air -gaps, figure 5 . The numerical model uses values of the flux linkage ($\Psi = \Phi N$), to predict the winding inductance as the armature moves. Both linear and non linear properties of the actuator cores are applied in this analysis. Figure 7 depicts the inductance functions in equations 11 and 12 and also illustrates the predicted inductance values from the numerical model.

Fig. 7. Inductance to the Air gap distance of a Single Energized Winding

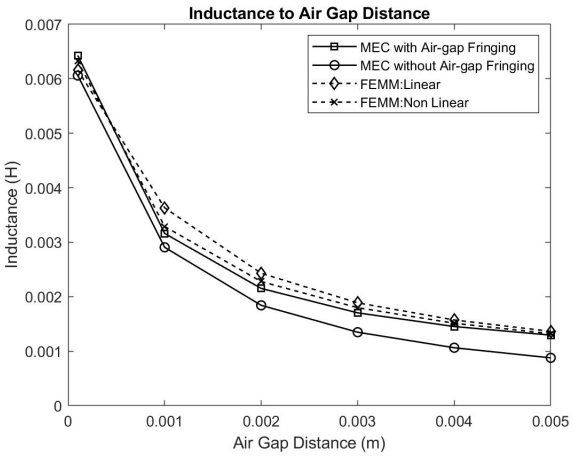

Considering figure 7, the models inductance increase as the variable air-gap distance decreases. The reluctance reduces as the air-gap closes and more energy is stored in the magnetic field, as a result an increase in inductance.The models have an inductance in the closed state (0.0001m) greater than the opened state (0.005m) [11].

The analytical model with fringing peaks higher than other models with an inductance of 0.0064H at a 100% stroke actuation. Major differences in the inductance values of the non linear FEMM model and the linear FEMM model do not occur till the armature has obtained 80% actuation. This is because saturation starts to occur in the non linear model's cores due to reduction in the reluctance [4].

Extras

One of the specifications of the analytical MEC model is the core properties must be linear. The ferromagnetic properties of both models, numerical and analytical, are similar, as shown in figure 8. The B-H curve illustrates Before saturation, all models follow a linear pattern. As the magnetic density reaches 1.5T, both MEC with Air-gap fringing follow is slight bend. This proves that air-gap fringing includes non linearity in the core material. Another model called the Nonlinear Magnetic Equivalent Circuit can also be used to show non-linearity in the core material[22].

Fig. 8. The B-H Curves of the Core Material

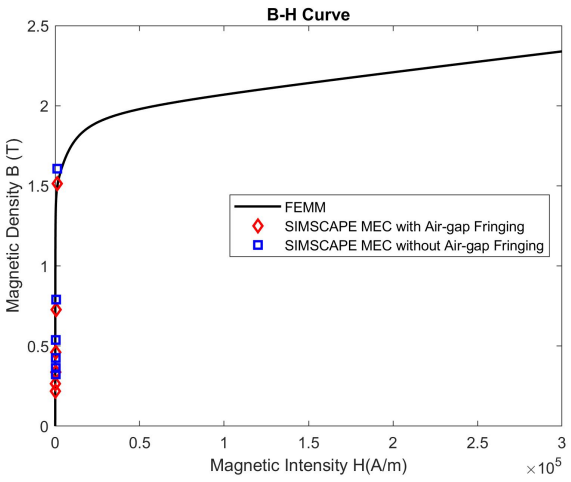

V. Forces on the Armature

Newtons laws of motion state that for a mass to be displaced, work needs to be done [11,14]. In the electromagnetic systems, the work done is analogous to the change in energy stored in the system, resulting in the displacement of the armature . The supply of current in the windings gives rise to motion in the armature. Flux is generated in the cores and passed through the air-gaps (figure 5). To estimate the Force that displaces the armature, the energy in the system must be accounted for[5,11].

The energy balance equation, assuming that losses (windings losses and core losses) are absent yields:

$$E_{electrical} = E_{mechanical} + E_{coupling} \tag{13}$$

As explained in section IV, the coupling field is the magnetic field. This can be written in the form of their individual work done.

$$\delta W_{electrical} = \delta W_{mechanical} + \delta W_{field} \tag{14}$$

Flux-linkage to Current ($\Psi - I$) Curves

Using a static process, the electrical energy, when there is no mechanical energy, i.e. no motion, is equivalent to the energy in the magnetic field. To analyse energy in the electric field, A flux-linkage to current curve is needed due Faraday's law [5,11]

$$E_{electrical} = \int IV\delta t = \int I\frac{\delta\Psi}{\delta t}\delta t = \int I\delta\Psi \tag{15}$$

This implies the energy in any stroke of the actuator, assuming no motion is:

$$\delta W_{elec} = \delta W_{field} = \int_0^{\Psi} I_\Psi \delta\Psi \tag{16}$$

In quasi-static process, The armature is assumed to move slowly. To determine the mechanical energy, the process is assumed to be dynamic. The excitation energy can be written in equation 17. The field, (equation 18), is not equivalent to the electric field due to the presence of the mechanical energy.

$$\delta W_{electrical} = \int_{\Psi_1}^{\Psi_2} I\delta\Psi \tag{17}$$

$$\delta W_{field} = \int_0^{\Psi_2} I_\Psi \delta\Psi - \int_0^{\Psi_1} I_\Psi \delta\Psi \tag{18}$$

where Ψ_1 and Ψ_2 are the flux-linkage values whose stroke actuation states ranges from 0% to 100%. In figures 9 and 10, the flux-linkage (Ψ) to current (I) characteristic for a **single winding** is illustrated. It shows for each air gap length, where 0% actuation implies 0.05m (open state) and 100%, 0.0001m (nominal value for closed state) . The analytical MEC models

Fig. 9. Flux-Linkage to current curves for Analytical Model (MEC) showing the different air-gap lengths

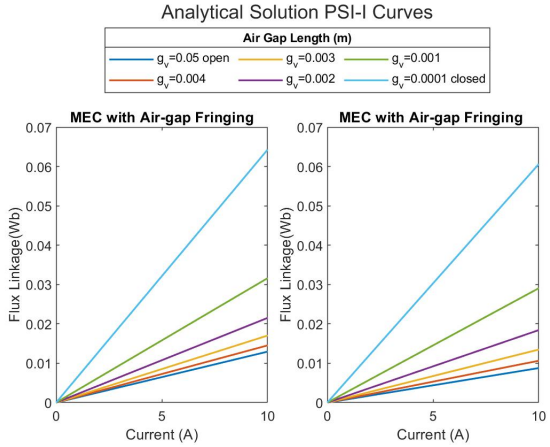

assume linearity in the cores of the actuator. The linearity supposes the flux permeating the cores is not sufficient to saturate it [11]. A 0.1 nominal closed value is assumed to ensure similarities in both models.

Fig. 10. Flux-Linkage to current curves for Finite Element Analysis Mode showing the different air-gap lengths

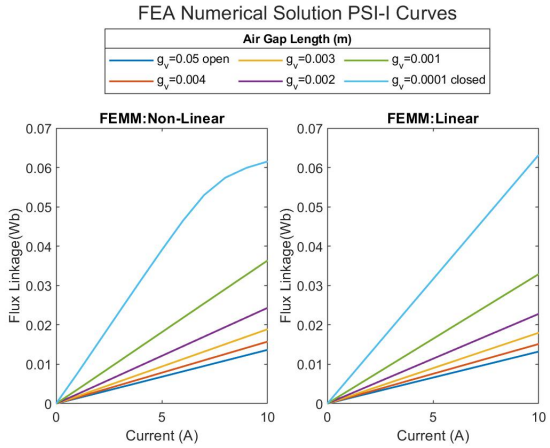

However, the FEMM model (10) illustrate both cases where saturation occurs and is absent. The output values are quite

similar except from the closed state when the flux supplied to the core is sufficient to saturate the ferromagnetic core, in the non linear sub-figure of 10.

Co-energy using $\Psi - I$ Curves

The $\Psi - I$ curves bound upper and lower areas in their plots. From equations 16 and 18, showing the magnetic in both static and dynamic operations. For static operations, the magnetic energy with respect to the $\Psi - I$ curves, show that the integral equations will be depend on the upper area. In magneto-static system, the energy stored in the magnetic field is equal to the lower area of the $\Psi - I$ curves, which is known as the Co-energy (E'_{field}) [11,14].

$$E'_{field} = \int_0^I \Psi_I \delta I \tag{19}$$

In dynamic systems, calculating the Mechanical Energy (E_{mech}) will require the Change in Co-energy ($\Delta E'_{field}$) [5]. It represents the difference between equations 17 and 18.

$$\Delta E'_{field} = \Delta E_{mech} = \int_{\Psi_1}^{\Psi_2} I\delta\Psi - \int_0^{\Psi_2} I_\Psi \delta\Psi + \int_0^{\Psi_1} I_\Psi \delta\Psi \tag{20}$$

In the actuator models, figures 11 and 12 represent the Mechanical energy in the systems. The values take into account the two windings by multiplying the Co-energy for a single winding by two. NOTE: The first point, on figures 11 and 12, represents the Co-energy at 0% actuation (there is no change in actuation) . In the FEA model,11, both linear

Fig. 11. Change in Co-energy Curves for Finite Element Analysis Model

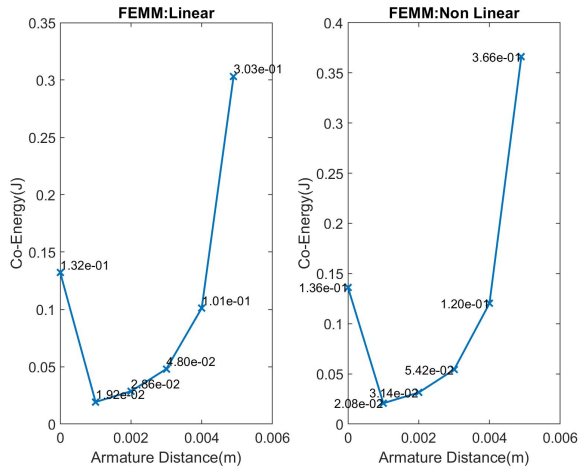

and non-linear subplots have nearly equal Co-energy before stroke movement. During movement, both curves still remain nearly equal with Non-linear having a slightly higher value at 100% actuation (0.005m). 'Unlike the FEA numerical model, the Analytical models,12, have larger differences in their values. The subplot with No magnetic fringing has lower value of Co-energy at 0% actuation.

Fig. 12. Change in Co-energy Curves for Analytical Model (MEC)

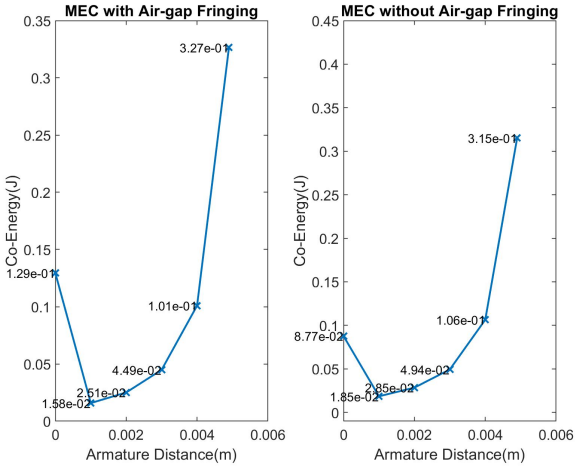

Methods of Calculating Change in Co-energy

In calculating the Co-energy of the FEMM model different methods can be used. One is using the $\Psi - I$ curve as explained in section V. Another way is the FEA model. This is by calculating the amount of Co-energy in the entire domain using the FEMM GUI. 5). The FEMM software uses equations of Magnetic density (B) and the field intensity (H) to predict the Co-energy in state of the actuator [1],21. It uses only the maximum excitation voltage to predict the amount of magnetic co-energy is enclosed in the elliptic boundaries. For non-linear ferromagnetic properties, the Change in Co-energy is given as taking p as the armature's initial position and $p + \partial$ as its final position:

$$\Delta E'_{field} = \left[\int \left(\int_0^H B(H')\delta H' \right) \delta V_w \right|_p^{p+\partial} \tag{21}$$

TABLE V
THE NON-LINEAR CHANGE IN CO-ENERGY CURVES USING THE METHODS OF CALCULATING CHANGE IN CO-ENERGY

Stroke	Change in Co-energy Methods (J)	
	$\Psi - I$ FEMM Curve(J)	FEA(J)
0%	0.1363	0.1362
20%	0.0208	0.0208
40%	0.0314	0.0314
60%	0.0542	0.0542
80%	0.1203	0.1202
100%	0.3661	0.3673

Using ∂ as 0.001m and p as 0m in equation 21, the values are compared with the $\Psi - I$ curve method, as shown in figure 13 and table V. There are slight differences in output results at 100% actuation because the $\Psi - I$ curve method assumes [14]:

1) All flux lines are confined to actuator geometry. Absence of leakage fluxes.

2) The core properties are linear.

The properties of the core is non linear which results to a difference when the core is saturating. The limitation of the $\Psi - I$ curve method is the boundary conditions approximated from the IABCs assumes an impedance in the unbounded region. This impedance produces a form of additional energy which affects the *'Circuit Properties'* [5] used to predict the flux linkage values [1]. The impedance value does not affect the FEA mode predictions because it is based on field and domain properties (B,H,and V_w) in the boundary.

Fig. 13. Change in Co-energy Curves showing $\Psi - I$ Curves and FEA model using Non-Linear properties

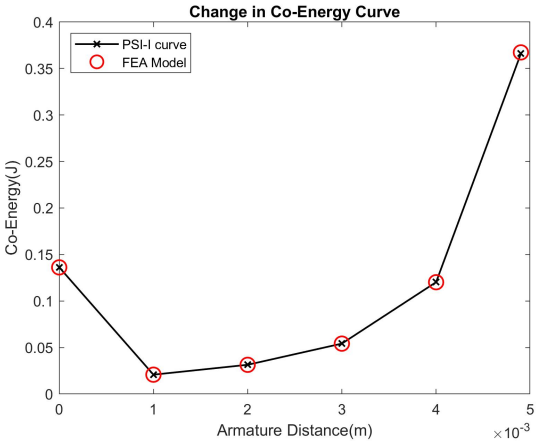

Forces

The force which moves the actuator is needed to estimate its behaviour of the sample. The relationship between the mechanical energy (E_{mech}) and force (F) can be given as:

$$E_{mech} = \int_{p}^{p+\partial} F(p)\delta p \tag{22}$$

Using equation numerical calculus principles [16] and the calculated E_{mech} in figures 11 and 12 result in a formula:

$$F(n) = \frac{E_{mech_n}}{\partial_n} \tag{23}$$

where $n \in [1, 6]$ and p_n represents the armature positions at n.

Figure 14 illustrates the Force displacement characteristic of the armature as it moves towards the stator, not the relationship with the air-gap. The initial position, when there is no displacement, 0m ,and final position of 0.005m. If figure 14 was a Force to air-gap curve, it would be down-slope instead of an up-slope [17].

The Force characteristic of the actuator is non-linear. The force acting on the armature exponentially increases as it moves closer to stator core. The FEMM Non-linear model peaks higher than other models because of the properties of the ferromagnetic material storing more energy when nonlinear. All other models assume linearity. They are more

Fig. 14. Force displacement Characteristic of the Actuator

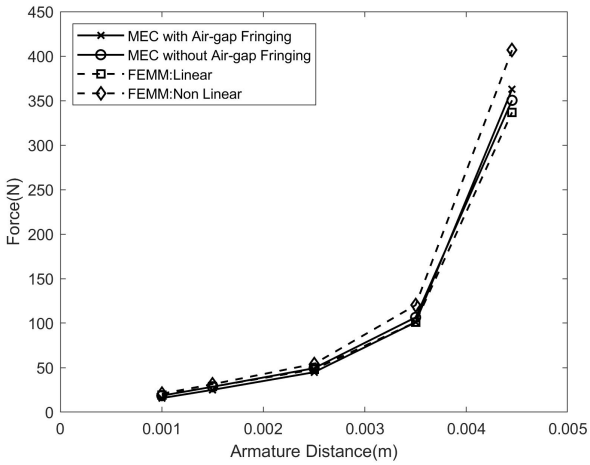

accurate in the force calculation, compared to the FEMM non-linear, because the $\Psi - I$ curve in calculating co-energy assumes for linear core properties.

VI. Comparison of Modelling Methods

From the analysis of the actuator, in calculating the Inductance, all models, excepting the model without fringing, at 0% stroke actuation have an initial inductance of approximately 0.0013H. These variations are because FEMM Models also account for fringing in the air-gaps [1] and the total reluctance of the model without fringing is greater that the models with fringing. The higher the reluctance the lesser the amount of inductance and therefore less energy at initial positions. The FEMM linear model has the least amount of force and energy at 100% actuation (figures 11 and 14). This is because the FEMM models do not assume the mean path of flux in it predictions unlike the analytical models. Instead they use the magnetic densities (B) around the core to predict their outputs which differ in the cores as illustrated 5.

There are a number of similarities between the FEMM models and the MEC models. Both operate similarly by observing Maxwell's laws and time invariance in their analysis [1-3,4]. Both models also use a 2-d model of the actuator sample. An advantage that FEMM models have over MEC models is testing for non-linearity of the core material as seen in different sections. The MEC models use only linear properties of actuator to approximate solutions. This is based on the assumption of Hopkins law, that limits the MEC model to electric circuit properties [11-13]. The flow of electricity in circuit is confined within the path of current and no leakage on lines. For this reason, the MEC model does not account for leakage flux which is present in magnetic circuits.

The numerical models use discretised mesh elements to predict the properties of the actuator. The disadvantage is that a high number of elements are needed for greater accuracy and precision of the output [2,7]. FEMM numerical analysis

involves the pre-processing, processing and post processing of the sample on it's interface [18,19]. This process is time consuming and requires enough storage space for outputs unlike analytical models [2].However, FEMM non linear model is the most accurate result because it accounts for real life properties of the actuator.

VII. CONCLUSION

In this paper, the technical specifications of the actuator sample were discussed and its estimated force output has a range 320N to 400N. The output's accuracy can be improved by using 3-d FEM or analytical models. The 3-d models include parts of the actuator in the directions of the plane and accounts for the true structure of the sample [10,20-21]. Thermal characterisation and Time varying models of the sample can also give more information about its behaviour, e.g velocity [11]. Another advancement is quantifying the magnetic losses in the system. Both models do not calculate the magnetic losses in the system. These are energy losses that occur as a result of the ferromagnetic properties and structure of the cores.The models used in electromagnetic characterisation prove that the design can be used in variety of operations. They include hysteresis, eddy's current and other core looses. In that sample, figure 1, a mechanical retaining system is absent [4]. Assuming the retaining system is a spring, the actuator can act as a electrically controlled valve [14]. In this application, the armature acts a plunger and motion can stop the flow of liquids. An example of an appliance it can be used is a fuel injection unit in vehicles. It can also be used in micro-actuation to aid motion of parts in robots.

REFERENCES

[1] D. Meeker. (2019) Finite element method magnetics (FEMM). [Online]. Available: www.FEMM.info

[2] B. Ladghem-Chikouche, K. Boughrara, F. Dubas and R. Ibtiouen, "2-d Semi-Analytical Magnetic Field Calculation for Flat Permanent-Magnet Linear Machines Using Exact Subdomain Technique," in IEEE Transactions on Magnetics, vol. 57, no. 6, pp. 1-11, June 2021.

[3] Chikouche, Brahim Ladghem, et al. "Two-dimensional hybrid model for magnetic field calculation in electrical machines: exact subdomain technique and magnetic equivalent circuit." COMPEL-The international journal for computation and mathematics in electrical and electronic engineering (2021).

[4] N. Simpson, "Electromagnetic characterisation of a short-stroke ferromagnetic actuator: Part a," 2019.

[5] N. Simpson, "Electromagnetic characterisation of a short-stroke ferromagnetic actuator: Part b," 2019.

[6] N. Simpson,; Mellor, Phil H. / Additive manufacturing of shaped profile windings for minimal AC loss in gapped inductors. 2017 IEEE International Electric Machines and Drives Conference (IEMDC 2017). Institute of Electrical and Electronics Engineers (IEEE), 2017.

[7] J. Shewchuck. A two-dimensional quality mesh generator and delaunay triangulator.triangle,. [Online].

[8] Loukas F. Kallivokas, Jacobo Bielak, Richard C. MacCamy,A simple impedance-infinite element for the finite element solution of the three-dimensional wave equation in unbounded domains, Computer Methods in Applied Mechanics and Engineering,Volume 147, Issues 3–4,1997,Pages 235-262,ISSN 0045-7825.

[9] K. Sugahara, "Improvised Asymptotic Boundary Conditions for Magnetostatic Field Problems in Ellipsoidal and Elliptic Cylindrical Domains," in IEEE Transactions on Magnetics, vol. 53, no. 6, pp. 1-4, June 2017.

[10] K. Sugahara,"Improvised Absorbing Boundary Conditions for three-dimensional electromagnetic finite elements," 2015 International Conference on Electromagnetics in Advanced Applications (ICEAA), 2015.

[11] N. Simpson and D. Drury, "Electro-mechanical energy conversion lecture notes," Lecture Notes, 2019.

[12] Jordan, D. W. "The Magnetic Circuit Model, 1850-1890: The Resisted Flow Image in Magnetostatics." The British Journal for the History of Science, vol. 23, no. 2, 1990, pp. 131–73, Accessed 11 Apr. 2022.

[13] Oner Y., Senol I., Bekiroglu N., Aycicek E. Magnetic equivalent circuit model of surface type fractional-slot permanent magnet synchronous generator. Journal of Vibroengineering, Vol. 15, Issue 1, 2013, p. 223-232.

[14] Giorgio Rizzoni. 2005. Fundamentals of Electrical Engineering. McGraw-Hill Science/Engineering/Math.

[15] E. Diller, S. Miyashita and M. Sitti, "Magnetic hysteresis for multi-state addressable magnetic microrobotic control," 2012 IEEE/RSJ International Conference on Intelligent Robots and Systems, 2012, pp. 2325-2331.

[16] Sozio, G. (2009). Numerical integration. Australian Senior Mathematics Journal, 23(1), 43-50.

[17] Vogel, O., Rair, R., lFe, R. (2011). Theory of Proportional Solenoids and Magnetic Force Calculation Using COMSOL Multiphysics.

[18] Sarac, Vasilija , Stefanov, Goce. (2011). Calculation of Electromagnetic Fields in Electrical Machines using Finite Elements Method. International Journal of Engineering and Industries. 2. 10.4156/ijei.vol2.issue1.3.

[19] Roylance, D. (2001). Finite element analysis. Department of Materials Science and Engineering, Massachusetts Institute of Technology, Cambridge.

[20] R. Dorget and T. Lubin, "Non-linear 3-D semi-analytical model for an axial flux reluctance magnetic coupling," in IEEE Transactions on Energy Conversion, doi: 10.1109/TEC.2022.3153173.

[21] Łukasz Skotny, L.S, (2020, March),"2D vs 3D Finite Element Analysis (with examples)", Available: https://enterfea.com/2d-vs-3d-finite-element-analysis/

[22] S. Mohammadi and M. Mirsalim, "Analytical Design Framework for Torque and Back-EMF Optimization, and Inductance Calculation in Double-Rotor Radial-Flux Air-Cored Permanent-Magnet Synchronous Machines," in IEEE Transactions on Magnetics, vol. 50, no. 1, pp. 1-16, Jan. 2014, Art no. 8200316, doi: 10.1109/TMAG.2013.2279129.